Received: 12 June 2017 | Accepted: 20 September 2017

DOI: 10.1111/jace.15257

ORIGINAL ARTICLE

Journal of the American Ceramic Society

# Liquid-phase sintering, microstructural evolution, and microwave dielectric properties of $Li_2Mg_3SnO_6$–LiF ceramics

**Ruzhong Zuo** | **Jian Zhang** | **Jie Song** | **Yudong Xu**

Institute of Electro Ceramics & Devices, School of Materials Science and Engineering, Hefei University of Technology, Hefei, China

**Correspondence**
Ruzhong Zuo, Institute of Electro Ceramics & Devices, School of Materials Science and Engineering, Hefei University of Technology, Hefei, China.
Email: rzzuo@hotmail.com

**Funding information**
The Anhui Provincial Natural Science Foundation of China, Grant/Award Number: 1508085JGD04

**Abstract**

The liquid-phase sintering behavior and microstructural evolution of $x$ wt% LiF aided $Li_2Mg_3SnO_6$ ceramics ($x$ = 1-7) were investigated for the purpose to prepare dense phase-pure ceramic samples. The grain and pore morphology, density variation, and phase structures were especially correlated with the subsequent microwave dielectric properties. The experimental results demonstrate a typical liquid-phase sintering in LiF–$Li_2Mg_3SnO_6$ ceramics, in which LiF proves to be an effective sintering aid for the $Li_2Mg_3SnO_6$ ceramic and obviously reduces its optimum sintering temperature from ~1200°C to ~850°C. The actual sample density and microstructure (grain and pores) strongly depended on both the amount of LiF additive and the sintering temperature. Higher sintering temperature tended to cause the formation of closed pores in $Li_2Mg_3SnO_6$-$x$ wt% LiF ceramics owing to the increase in the migration ability of grain boundary. An obvious transition of fracture modes from transgranular to intergranular ones was observed approximately at $x$ = 4. A single-phase dense $Li_2Mg_3SnO_6$ ceramic could be obtained in the temperature range of 875°C-1100°C, beyond which the secondary phase $Li_4MgSn_2O_7$ (<850°C) and $Mg_2SnO_4$ (>1100°C) appeared. Excellent microwave dielectric properties of $Q \times f$ = 230 000-330 000 GHz, $\varepsilon_r$ = ~10.5 and $\tau_f$ = ~−40 ppm/°C were obtained for $Li_2Mg_3SnO_6$ ceramics with $x$ = 2-5 as sintered at ~1150°C. For LTCC applications, a desirable $Q \times f$ value of ~133 000 GHz could be achieved in samples with $x$ = 3-4 as sintered at 875°C.

KEYWORDS

densification, dielectric materials/properties, grain growth, LTCC, sinter/sintering

## 1 | INTRODUCTION

The past few decades have witnessed tremendous development of wireless communications in mobile phone and satellite communication systems. Dielectrics with a high quality factor $Q \times f$ value (>100 000 GHz) and a relatively low dielectric permittivity ($\varepsilon_r < 20$) have attracted much attention in microwave circuit, substrates, and passive components. In order to fulfill the requirement of the low-temperature co-fired ceramics (LTCC) technology, the dielectrics should be well sintered below 950°C to cofire with Ag.[1,2] Nowadays, extensive research has been also carried out on ultralow-temperature cofired ceramics with sintering temperatures of less than 700°C, such as glass-ceramics, molybdates, vanadates, tungstates, tellurates-based ceramics, etc.[3-5]

Rock salt-structured $Li_2MO_3$ (M = Ti, Sn, Zr) ceramics have been extensively investigated in recent years. However, their possible practical applications in LTCC were restricted by relatively high sintering temperatures (>1200°C).Porous microstructures might be common shortcomings for Li-based compounds because the Li volatilization becomes serious at high temperatures, although some modifications were made by forming solid solutions with ZnO, MgO or NiO.[6-8] Moreover, Li-based $Li_2Mg_3MO_6$ ceramics with a similar rock salt structure have also received increasing attention.[9-11] These ceramics sintered at 1280°C-1380°C possessed excellent microwave dielectric properties of $\varepsilon_r = 15.2$, 8.8, and 12.6, $Q \times f = 152\,000$, 123 000 and 86 000 GHz, and temperature coefficient of resonance frequency $\tau_f = -39$, $-32$ and $-36$ ppm/°C, respectively.[9] However, the second phases $Mg_2SnO_4$ and $ZrO_2$ occurred in $Li_2Mg_3SnO_6$ and $Li_2Mg_3ZrO_6$ ceramics, respectively, as a result of the lithium evaporation at high sintering temperatures. Therefore, lowering the sintering temperature and achieving dense and even microstructure might be the key issues to improve electrical properties of $Li_2Mg_3MO_6$ ceramics. In our previous work, ultrahigh-$Q$ $Li_{2(1+x)}Mg_3ZrO_6$ microwave dielectric ceramics were successfully prepared by means of Li-rich atmosphere-controlled sintering.[12] The result showed that both well-sintered ceramics and suppressed secondary phases contributed to low-loss microwave dielectric ceramics with $Q \times f$ values of 150 000-300 000 GHz. $Li_2Mg_3SnO_6$ ceramics have the same crystal structure as $Li_2Mg_3ZrO_6$. By contrast, the relevant research of the latter is extremely rare. The foreseeable potentials of $Li_2Mg_3SnO_6$ ceramics should be expected if dense $Li_2Mg_3SnO_6$ ceramics can be prepared.

Liquid phase sintering is generally believed to be one of the most effective and least expensive ways of achieving high-density ceramics at a relatively low sintering temperature. An ideal sintering aid should effectively lower the sintering temperature and simultaneously maintain the electrical properties as much as possible. The densification behavior of $Li_2TiO_3$ ceramics could be significantly improved by adding $Li_2CO_3$,[13] $H_3BO_3$,[14] $ZnO–B_2O_3$,[15] $B_2O_3–CuO$,[16] $Li_2WO_4$ ($\varepsilon_r = 5.5$, $Q \times f = 62\,000$ GHz, and $\tau_f = -146$ ppm/°C as sintered at 650°C),[17,18] etc. Low-melting-point fluorides were also used as sintering fluxes in many ceramic systems, such as rock salts,[19-21] perovskites,[22,23] spinels,[24,25] silicates,[26] etc. Either a traditional liquid phase sintering or a transient liquid phase sintering was proposed in these previous studies. However, no obvious evidences were provided to support statements concerning the proposed sintering mechanisms, in which the evolution of microstructure should be especially involved. Particularly, how the microstructure evolution influenced the final dielectric properties was still unknown, considering that it might be related to both sintering temperature and the additive content in a special liquid-phase sintering case. In current work, a dense and phase-pure $Li_2Mg_3SnO_6$ ceramic with excellent microwave dielectric properties was successfully manufactured by means of a small amount of LiF. Most importantly, the microwave dielectric properties were well interpreted by means of not only the sample density variation with sintering temperature and the LiF content, but also the evolving grain and pore morphology, through which a LiF-aided liquid-phase sintering mechanism was discussed in detail.

## 2 | EXPERIMENTAL PROCEDURE

$Li_2Mg_3SnO_6$-$x$ wt% LiF ($x = 1$-7) ceramics were prepared by a conventional solid-state route. $Li_2CO_3$ (98.0%), MgO (98.5%), $SnO_2$ (99.0%), and LiF (99.6%) (Sinopharm Chemical Reagent Co. Ltd., Shanghai, China) powders were used as starting materials. Stoichiometric amounts of raw powders were weighed according to the formula of $Li_2Mg_3SnO_6$. The powder mixtures were first milled with $ZrO_2$ balls in alcohol for 4 hours and then calcined at 1000°C for 8 hours in air after drying. The as-synthesized $Li_2Mg_3SnO_6$ and LiF powders at different weight ratios were ball-milled for 6 hours again, then granulated with 5 wt% PVA binder, and finally uniaxially pressed into cylinders with dimensions of 10 mm in diameter and 5-6 mm in height under a uniaxial pressure of ~200 MPa. These samples were heated at 550°C for 4 hour to burn out the organic binder, and then sintered in air in the temperature range from 800°C to 1300°C for 6 hours at a heating rate of 5°C/min.

The apparent density of the sintered specimens was measured using the Archimedes method. The crystalline phases were identified by an X-ray diffractometer (XRD; D/Max2500V, Rigaku, Tokyo, Japan) over 10°-90° at a step of 0.02°. Prior to the examination, the sintered pellets were crushed into powders with an agate mortar. The microstructure observation on the fractured surfaces of the sintered pellets was performed using a field-emission scanning electron microscope (FE-SEM; SU8020, JEOL, Tokyo, Japan) coupled with an energy dispersive spectroscope (EDS). Microwave dielectric properties of well-polished samples with an aspect ratio of 1.8-2.2 were evaluated with a network analyzer (Agilent, N5230C, Palo Alto, CA) and a temperature chamber (GDW-100, Saiweisi, Changzhou, China) by means of a Hakki-Coleman post resonator method.[27] The dielectric permittivity $\varepsilon_r$ was measured using the parallel conducting plates and the coaxial electric probes as suggested by Courtney at the $TE_{011}$ mode of resonance, which can be least perturbed by the surrounding field variation. All measurements were performed at room temperature in the frequency of 8-12 GHz. The $\tau_f$ value of the samples was measured by noting the change in the resonant frequency over a temperature interval from 25°C to 80°C, as calculated by the following equation: $\tau_f = (f_2 - f_1)/(f_1(T_2 - T_1))$, where $f_1$ and $f_2$ represent the resonant frequencies at $T_1$ and $T_2$, respectively.

## 3 | RESULTS AND DISCUSSION

The XRD patterns of as-calcined $Li_2Mg_3SnO_6$ powders and as-sintered $Li_2Mg_3SnO_6$-$x$ wt% LiF crushed samples are displayed in Figures 1A,B, respectively. On the one hand, all main diffraction peaks of the calcined powder ($x = 0$) could be well indexed to the standard pattern of a cubic $Li_2Mg_3SnO_6$ (JCPDS #39-0932). A small broad peak near 20° can be faintly observed for the calcined powder. This peak seemed to become obvious when the $x = 1$ $Li_2Mg_3SnO_6$ sample was sintered at 1200°C. The secondary phase should be $Mg_2SnO_4$ by comparing its diffraction peaks with the standard pattern (JCPDS #74-2152). This might result from the lithium volatilization in the matrix composition at a relatively high sintering temperature.[9] The results indicated that the addition of LiF could not effectively provide Li-rich sintering atmosphere, which was different from the addition of $Li_2CO_3$.[12,13] By comparison, ceramic samples with 2-4 wt% LiF sintered at their optimum temperatures owned a pure cubic $Li_2Mg_3SnO_6$ phase (JCPDS #39-0932). The increase in LiF content tended to obviously decrease the optimum sintering temperature of $Li_2Mg_3SnO_6$ samples, so that the lithium volatilization was suppressed at a relatively low sintering temperature. On the other hand, as compared with the standard pattern (JCPDS #37-1164), a little $Li_4MgSn_2O_7$ secondary phase was found to appear along with the main phase $Li_2Mg_3SnO_6$ in the $x = 7$ composition sintered at 850°C. The possible reason might be that $Li_4MgSn_2O_7$ tended to precipitate from $Li_2Mg_3SnO_6$ at relatively low temperatures. In the binary phase diagram of $Li_2SnO_3$–MgO,[28] there exists a transition from $Li_4MgSn_2O_7$ to $Li_2Mg_3SnO_6$ at ~800°C-850°C.

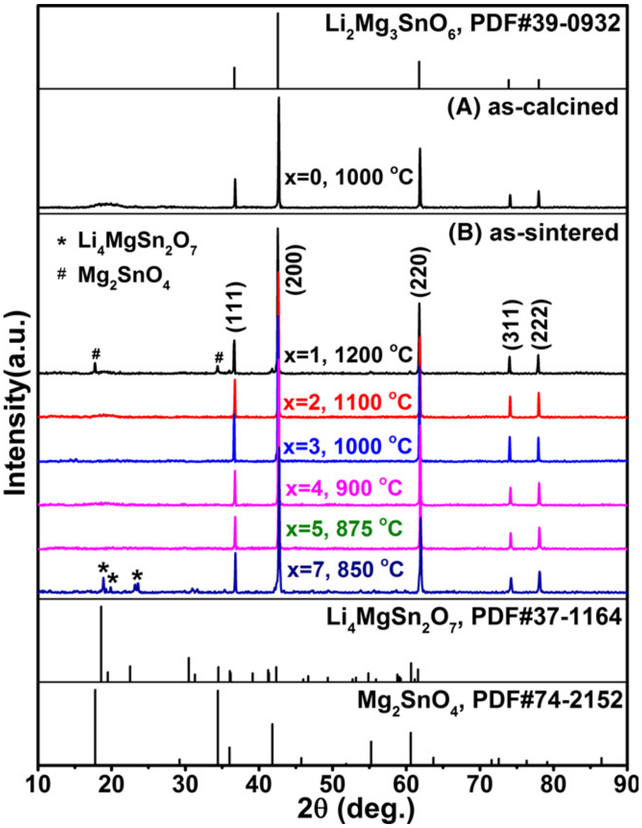

**FIGURE 1** XRD patterns of (A) $Li_2Mg_3SnO_6$ powders calcined at 1000°C for 8 hours and (B) crushed $Li_2Mg_3SnO_6-x$ wt% LiF samples sintered at their optimum temperatures, as compared with the standard patterns of $Li_2Mg_3SnO_6$, $Li_4MgSn_2O_7$ and $Mg_2SnO_4$ [Color figure can be viewed at wileyonlinelibrary.com]

Although the LiF content was increased in a wide content range, the secondary phase was not detected, probably meaning that no chemical reaction occurred between LiF and the matrix. In LiF-added $Li_2Mg_3TiO_6$ ceramics, LiF was believed to diffuse into the lattice of $Li_2Mg_3TiO_6$ during sintering.[20] However, a detectable diffraction peak shift was not observed in $Li_2Mg_3SnO_6$-$x$ wt% LiF ceramics, as can be seen in Figure 1B. Therefore, we believed that LiF formed a liquid phase at higher temperatures and acted as a sintering aid during densification process, and then probably existed in the sample in the form of noncrystalline phases at room temperature. This can be further confirmed infra. As a result, the as-observed secondary phases such as $Li_4MgSn_2O_7$ (lower temperatures) or $Mg_2SnO_4$ (higher temperatures) were mainly caused by different sintering temperatures, irrespective of LiF itself. For sintered $Li_2Mg_3SnO_6$-$x$ wt% LiF samples, the $Mg_2SnO_4$ secondary phases always appeared as sintering temperature was higher than 1150°C, but disappeared as sintering temperature was lower than 1100°C, as shown in Figure 2. According to the above analysis, it is clear that the $Li_2Mg_3SnO_6$ sample needs to be well densified in the temperature range of 850°C-1100°C in order to prepare pure-phase ceramics (aside from noncrystalline phases from sintering aids).

The apparent density and $\varepsilon_r$ of $Li_2Mg_3SnO_6$-$x$ wt% LiF ceramics sintered at various temperatures are shown in Figure 3A. As sintering temperature increased, the sample density firstly increased to their respective maximum values and then tended to decrease with further increasing sintering temperature. The optimum sintering temperatures of the specimens decreased from 1200°C to 850°C with increasing the amount of LiF from $x = 1$ to $x = 3$. A further increase in the LiF content did not obviously decrease the optimum sintering temperature any more. Moreover, the maximum apparent density was reached approximately at $x = 4$. These results indicated that the amount of the produced liquid phases at $x = 3$ or $x = 4$ should be enough to ensure the liquid-phase sintering mechanism for $Li_2Mg_3SnO_6$ samples. As expected, the overmuch liquid phase proved to be disadvantage against the sintering of the sample, leading to a decline of the sample density. Generally, $\varepsilon_r$ mainly depends on the density, ionic

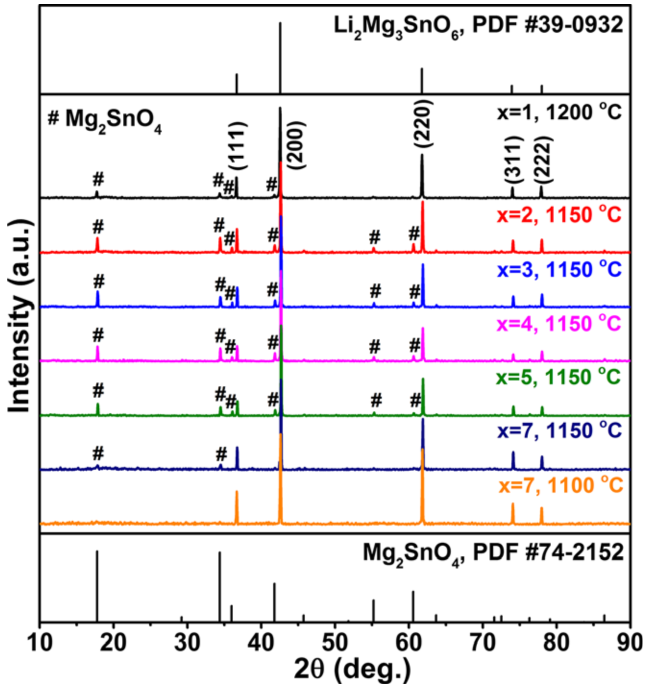

**FIGURE 2** XRD patterns of $Li_2Mg_3SnO_6$−$x$ wt% LiF samples sintered at different temperatures from 1100°C-1200°C as indicated [Color figure can be viewed at wileyonlinelibrary.com]

polarizability, microstructure, porosity, and secondary phase.[29] The $\varepsilon_r$ values of $Li_2Mg_3SnO_6$-$x$ wt% LiF ceramic sintered at different temperatures are shown in Figure 3B. The variation in $\varepsilon_r$ with sintering temperature presented a similar trend to that of the sample density. For the same composition, a rapid decrease in $\varepsilon_r$ at higher temperatures particularly than 1100°C, should be partially ascribed to the emergence of the secondary phase $Mg_2SnO_4$ with a smaller $\varepsilon_r$ of ~8.4.[30] At the same sintering temperature, the difference in $\varepsilon_r$ should be mainly attributed to the sample density and the glass phases. For the $x = 7$ sample, the $\varepsilon_r$ value was found to be relatively low although it seemed to have a similar apparent density to samples with $x = 3$-5. Aside from the possible difference in the glass phase content, the above results might be also related to the special microstructure as discussed infra.

Figure 4 shows the fracture morphology of $Li_2Mg_3SnO_6$-$x$ wt% LiF ceramics sintered at their respective optimum sintering temperatures and higher temperatures. First of all, the fracture modes of the ceramic samples were found to change from transgranular ones ($x \le 3$) to intergranular ones ($x > 3$) with increasing the LiF content. Secondly, the grain size was found to exhibit a rapid drop from ~8 μm at $x = 1$ (1200°C) to 0.65 μm at $x = 7$ (850°C). At the same sintering temperature (for example at 1200°C), the grain size was also increased with increasing the LiF content. This result indicated that the grain growth is sensitive to both the sintering temperature and the amount of the liquid phase during a liquid-phase sintering. As $x < 3$, the optimum sintering temperature of the sample was still higher than 1100°C probably owing to the insufficient liquid phase. Higher sintering temperatures would speed up the migration of grain boundaries so that the driving force of sintering became much smaller. As a result, a lot of pores remained on the triple junctions (as indicated by blue arrows, open pores) in addition to a few pores trapped in the interior of grains (as indicated by red arrows, closed pores) for the $x = 1$ and $x = 2$ samples. The formation of closed pores would impede the progress of sintering process, leading to a rather low density for the $x = 1$ and $x = 2$ samples. The appearance of closed pores during liquid-phase sintering would be favored as sintering temperature increased, as can be seen if one compared Figure 4(A and G), 4(B and H), 4(C and I), as well as Figure 4(D and J). It was usually accompanied by a rapid grain growth (see Figures 4G-J) because the enhanced migration ability of grain boundary at higher temperatures allows it to overcome the pinning effect of small pores. This situation started to be improved as $x = 3$, so that the sample density was greatly increased at its optimum sintering temperature (1000°C). Most obviously, the $x = 4$ sample sintered at 900°C exhibited very dense microstructure (nearly indiscernible pores) and medium grain growth (~4 μm in grain size), which is probably attributed to both lower sintering temperature and appropriate amount of sintering aid LiF. For $x \ge 4$ samples sintered at their optimum temperatures, an obvious intergranular fracture was observed probably because of the increased amount of grain-boundary phases. However, the $x = 4$ sample was still transgranularly fractured as it was sintered at 1200°C (see Figure 4J), in which large grain sizes and closed pores are observed. Although none of any closed pores could be

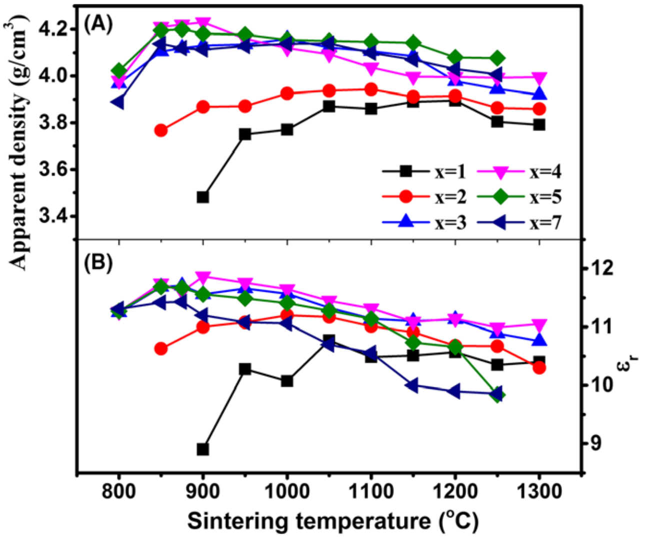

**FIGURE 3** (A) Apparent density and (B) $\varepsilon_r$ of $Li_2Mg_3SnO_6$−$x$ wt% LiF ceramics sintered at different temperatures [Color figure can be viewed at wileyonlinelibrary.com]

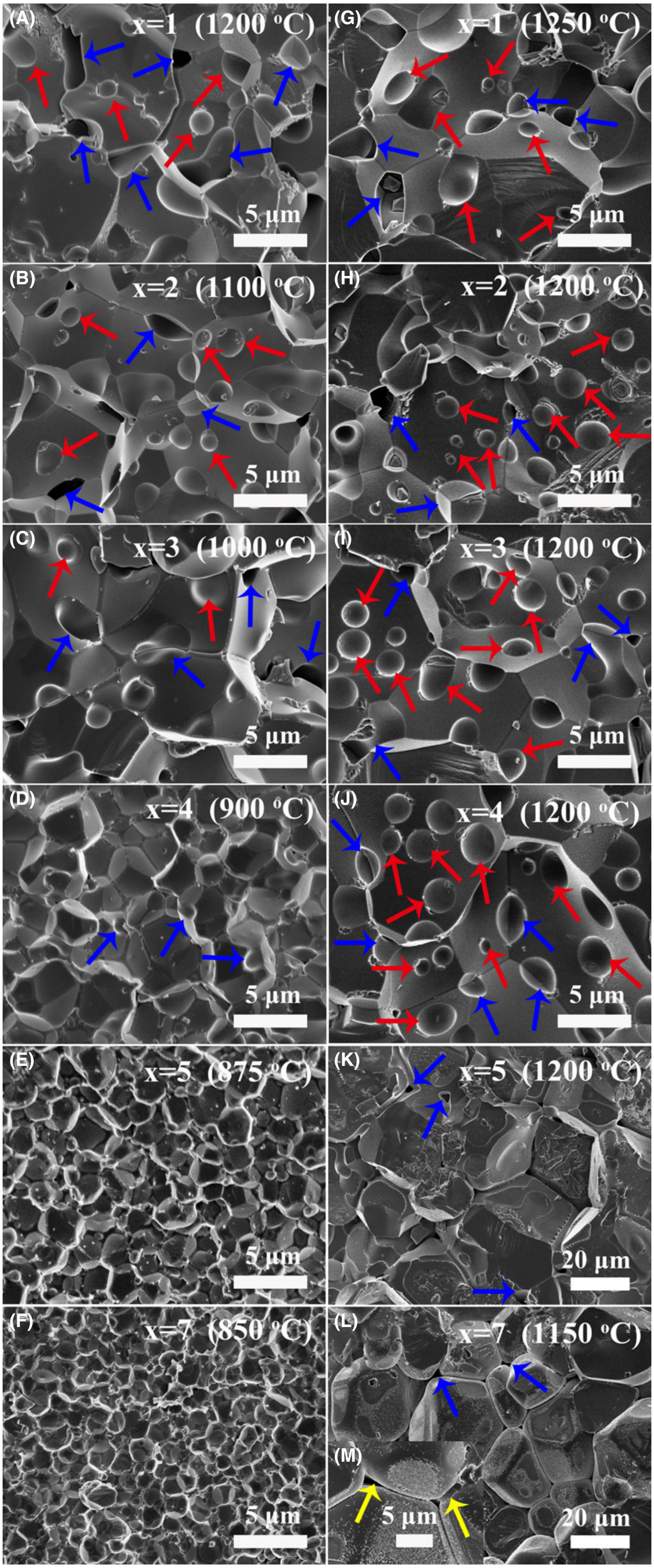

**FIGURE 4** SEM images on fractured surfaces of $Li_2Mg_3SnO_6-x$ wt% LiF ceramics sintered at (A-F) their optimum temperatures and (G-L) higher temperatures as indicated. The inset (*m*) shows the locally magnified grain boundary region in (L). The blue, red, and yellow arrows schematically stand for intergranular pores (open pores), intracrystalline pores (closed pores), and grain-boundary gaps (phases), respectively [Color figure can be viewed at wileyonlinelibrary.com]

observed from the fracture image of the $x = 5$ and $x = 7$ samples as they were sintered at 1150°C-1200°C, yet the grain size became extremely large. The extremely large grains should usually accompany the formation of closed pores, as similarly observed in Figure 4J. Closed pores were not observed in the fractured morphology of the $x = 5$ or $x = 7$ sintered at higher temperatures most probably because of intergranular fracture modes for these two compositions. The formation of intergranular fracture modes should be closely related to the weakening of the grain boundary strength owing to increasing amount of grain-boundary glass phases, as can be seen in the inset (M) of Figure 4L (as indicated by yellow arrow). The shrinkage effect during solidifying of liquid phase would also lead to the formation of the crevice between two grains.

Figure 5 illustrates the $Q \times f$ value of $Li_2Mg_3SnO_6$-$x$ wt% LiF ceramics sintered at different temperatures. It can be seen that there were two $Q \times f$ peak values approximately near 850°C and 1150°C for different compositions. It is noteworthy that the variation in the $Q \times f$ value with sintering temperature was much more complicated than the variation in either density or $\varepsilon_r$. In the higher temperature region, most of compositions first exhibited a gradual increase in $Q \times f$ values with increasing temperature, then reached their maximum values of 230 000-330 000 GHz at ~1150°C and finally started to decrease rapidly with further increasing temperature. By comparison, the maximum $Q \times f$ values for the $x = 1$ and $x = 7$ samples appeared at 1200°C and 1100°C, respectively, probably because of different LiF contents. The maximum $Q \times f$ value for the $x = 7$ sample at 1100°C was relatively low, probably because of a large amount of noncrystalline grain-boundary phases. Interestingly, in the temperature range of 1000°C-1150°C where $Q \times f$ values gradually increased, the sample density for most of samples did not increase with increasing temperature (see Figure 3). As a result, the increase in $Q \times f$ values might be partially attributed to the grain growth with sintering temperature, as can be seen from Figure 4. The additional important reason might be related with the appearance of secondary phase $Mg_2SnO_4$ (see Figure 2). Therefore, it is speculated that the secondary phase $Mg_2SnO_4$ might be beneficial to the $Q \times f$ value of the matrix although microwave dielectric properties of the single-phase $Mg_2SnO_4$ have not been reported for its difficulty in synthesis.[30] A rapid decline of $Q \times f$ values after ~1150°C should be attributed to the increased amount of closed pores with increasing temperature,[31] as can be seen from Figure 4. That is to say, although the apparent density of the sample did not decrease rapidly, the actual sample density was much lower than the Archimedes density because closed pores were not taken into account in the measurement. Besides, the glass phase existing in the sintered samples might be another reason for the decrease in $Q \times f$ value, as shown by yellow arrows in Figure 4M.

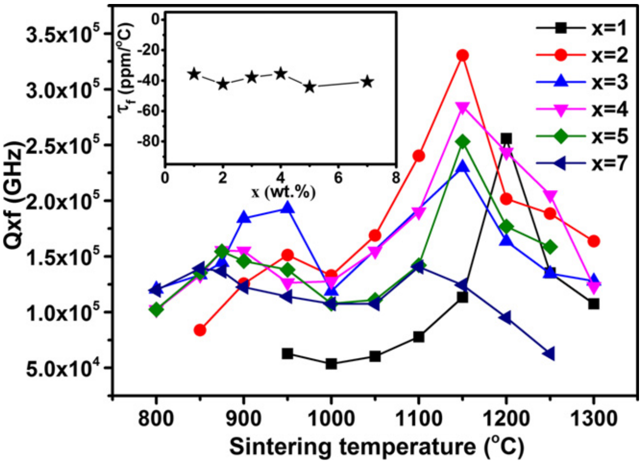

**FIGURE 5** $Q \times f$ values of $Li_2Mg_3SnO_6-x$ wt% LiF ceramics sintered at different temperatures. The inset shows $\tau_f$ values of $Li_2Mg_3SnO_6-x$ wt% LiF ceramics sintered at optimum temperatures [Color figure can be viewed at wileyonlinelibrary.com]

Furthermore, in the lower temperature region (800°C-1000°C), the $Q \times f$ value of each sample exhibited a peak value. The temperature points for the $Q \times f$ peak values were found to slightly decrease with increasing the LiF content, and they seemed slightly lower than their corresponding optimum sintering temperatures, probably owing to the same fact that the closed pores made the measured density lower than the actual density. A relatively large $Q \times f$ value of ~193 000 GHz was observed in the $x = 3$ sample sintered at ~950°C. For LTCC applications, a desirable $Q \times f$ value of ~133 000 GHz could be achieved in the samples with $x = 3$ and $x = 4$ as they were sintered at 875°C, basically being attributed to the dense body, phase purity, and uniform microstructure. The decrease in $Q \times f$ values with further decreasing sintering temperature might be due to the lowering of the sample density. The influence of the secondary phase $Li_4MgSn_2O_7$ on the $Q \times f$ value below 850°C was unknown because there were no reference data reported. The inset of Figure 5 shows $\tau_f$ values of $Li_2Mg_3SnO_6$-$x$ wt% LiF ceramics sintered at their optimum sintering temperatures. It can be seen that the $\tau_f$ value remained in a narrow range of −35-−42 ppm/°C for different compositions, meaning that it is not sensitive to the variation in the density and microstructure compared to the $Q \times f$ value.

## 4 | CONCLUSIONS

The effect of LiF addition on the sintering behavior, phase structure, microstructure and microwave dielectric properties of $Li_2Mg_3SnO_6$ ceramics was investigated in detail. The results indicate that LiF effectively promoted the sintering of $Li_2Mg_3SnO_6$ ceramics by means of a liquid-phase sintering mechanism. The actual sample density and microstructure (grain and pores) strongly depended on both the amount of LiF additive and the sintering temperature. Higher sintering temperature tended to increase the migration ability of grain boundary, leading to the formation of closed pores in $Li_2Mg_3SnO_6$-$x$ wt% LiF ceramics. With increasing the amount of LiF, the ceramic sample exhibited an obvious transition from the transgranular to intergranular fracture. A single-phase $Li_2Mg_3SnO_6$ ceramic could be obtained in the temperature range of 875°C-1100°C, beyond which the secondary phase $Li_4MgSn_2O_7$ (<850°C) and $Mg_2SnO_4$ (>1100°C) appeared. Excellent microwave dielectric properties of $Q \times f$ = 230 000-330 000 GHz, $\varepsilon_r$ = ~10.5 and $\tau_f$ = ~−40 ppm/°C were attained for $Li_2Mg_3SnO_6$ ceramics with $x$ = 2-5 as sintered at ~1150°C. By comparison, a desirable $Q \times f$ value of ~133 000 GHz could be achieved in samples with $x$ = 3-4 as they were sintered at 875°C, which might be suitable for LTCC applications.

## ACKNOWLEDGMENTS

Financial support from the Anhui Provincial Natural Science Foundation (1508085JGD04) is gratefully acknowledged.

## ORCID

*Ruzhong Zuo* http://orcid.org/0000-0001-8295-4323

## REFERENCES

1. Sebastian MT, Jantunen H. Low loss dielectric materials for LTCC applications: a review. *Int Mater Rev*. 2008;53:57-90.
2. Narang SB, Bahel S. Low loss dielectric ceramics for microwave applications: a review. *J Ceram Process Res*. 2010;11:316-321.
3. Sebastian MT, Wang H, Jantunen H. Low temperature co-fired ceramics with ultra-low sintering temperature: a review. *Curr Opin Solid State Mater Sci*. 2016;20:151-170.
4. Zhou D, Randall CA, Wang H, et al. Microwave dielectric ceramics in $Li_2O$–$Bi_2O_3$–$MoO_3$ system with ultra-low sintering temperatures. *J Am Ceram Soc*. 2010;93:1096-1100.
5. Zhou H, Miao Y, Chen J, et al. Sintering characteristic, crystal structure and microwave dielectric properties of a novel thermally stable ultralow firing $Na_2BiMg_2V_3O_{12}$ ceramic. *J Mater Sci Mater Electron*. 2014;25:2470-2474.
6. Bian JJ, Dong YF. New high Q microwave dielectric ceramics with rock salt structures: $(1-x)Li_2TiO_3 + xMgO$ system ($0 \le x \le 0.5$). *J Eur Ceram Soc*. 2010;30:325-330.
7. Huang CL, Tseng YW, Chen JY. High-Q dielectrics using ZnO-modified $Li_2TiO_3$ ceramics for microwave applications. *J Eur Ceram Soc*. 2012;32:3287-3295.
8. Zhang J, Zuo RZ. Low-temperature fired thermal-stable $Li_2TiO_3$–NiO microwave dielectric ceramics. *J Mater Sci Mater Electron*. 2016;27:7962-7968.
9. Fu Z, Liu P, Ma J, et al. Novel series of ultra-low loss microwave dielectric ceramics: $Li_2Mg_3BO_6$ (B = Ti, Sn, Zr). *J Eur Ceram Soc*. 2016;36:625-629.
10. Wu H, Kim ES. Correlations between crystal structure and dielectric properties of high-Q materials in rock-salt structure $Li_2O$–MgO–$BO_2$ (B = Ti, Sn, Zr) systems at microwave frequency. *RSC Adv*. 2016;6:47443-47453.
11. Zhou H, Tan X, Huang J, et al. Sintering behavior, phase evolution and microwave dielectric properties of thermally stable $Li_2O$–3MgO–m$TiO_2$ ceramics ($1 \le m \le 6$). *Ceram Int*. 2017;43:3688-3692.
12. Song J, Zhang J, Zuo RZ. Ultrahigh *Q* values and atmosphere-controlled sintering of $Li_{2(1+x)}Mg_3ZrO_6$ microwave dielectric ceramics. *Ceram Int*. 2017;43:2246-2251.
13. Bian JJ, Dong YF. Sintering behavior, microstructure and microwave dielectric properties of $Li_{2+x}TiO_3$ ($0 \le x \le 0.2$). *Mater Sci Eng, B*. 2011;176:147-151.
14. Liang J, Lu WZ, Wu JM, et al. Microwave dielectric properties of $Li_2TiO_3$ ceramics sintered at low temperatures. *Mater Sci Eng, B*. 2011;176:99-102.
15. Liang J, Lu WZ. Microwave dielectric properties of $Li_2TiO_3$ ceramics doped with ZnO–$B_2O_3$ frit. *J Am Ceram Soc*. 2009;92:952-954.
16. Pang LX, Zhou D. Microwave dielectric properties of low-firing $Li_2MO_3$ (M = Ti, Zr, Sn) ceramics with $B_2O_3$–CuO addition. *J Am Ceram Soc*. 2010;93:3614-3617.
17. Wang Z, Song L, Bian JJ. Low temperature sintering and microwave dielectric properties of $Li_2TiO_3$–$Li_2WO_4$ composite ceramics. *Ceram Int*. 2013;39:9767-9772.
18. Zhou D, Randall CA, Pang LX, et al. Microwave dielectric properties of $Li_2WO_4$ ceramic with ultra-low sintering temperature. *J Am Ceram Soc*. 2011;94:348-350.
19. Ding Y, Bian JJ. Structural evolution, sintering behavior and microwave dielectric properties of $(1-x)Li_2TiO_3 + x$LiF ceramics. *Mater Res Bull*. 2013;48:2776-2781.
20. Fu Z, Liu P, Ma J, et al. New high *Q* low-fired $Li_2Mg_3TiO_6$ microwave dielectric ceramics with rock salt structure. *Mater Lett*. 2016;164:436-439.
21. Mao YX, Pan HL, Zhang YW, et al. Effects of LiF addition on the sintering behavior and microwave dielectric properties of $Li_2Mg_3SnO_6$ ceramics. *J Mater Sci Mater Electron*. 2017;28:13278-13282.
22. Yang WG, Zhang BP, Ma N, et al. High piezoelectric properties of $BaTiO_3$–$x$LiF ceramics sintered at low temperatures. *J Eur Ceram Soc*. 2012;32:899-904.
23. Zhou JJ, Cheng LQ, Wang K, et al. Low-temperature sintering of (K, Na)$NbO_3$-based lead-free piezoceramics with addition of LiF. *J Eur Ceram Soc*. 2014;34:1161-1167.
24. Sutorik AC, Gilde G, Cooper C, et al. The effect of varied amounts of LiF sintering aid on the transparency of alumina rich spinel ceramic with the composition MgO $1.5Al_2O_3$. *J Am Ceram Soc*. 2012;95:1807-1810.
25. Yang Z, Wang B, Ren Y, et al. Densification behavior, microstructure, mechanical and optical properties of Mg-doped sialon with fluoride additives. *J Eur Ceram Soc*. 2017;37:1985-1992.

26. Zhang J, Yue Z, Luo Y, et al. Novel low-firing forsterite-based microwave dielectric for LTCC applications. *J Am Ceram Soc*. 2016;99:1122-1124.
27. Hakki BW, Coleman PD. A dielectric resonator method of measuring inductive capacities in the millimeter range. *IEEE Trans Microwave Theory Technol*. 1960;8:402-410.
28. Castellanos M, West AR. Compound and solid solution formation in the system, $Li_2SnO_3$–MgO. *J Mater Sci Lett*. 1984;3:786-788.
29. Liao QW, Li LX, Ren X, et al. New low-loss microwave dielectric material $ZnTiNbTaO_8$. *J Am Ceram Soc*. 2011;94:3237-3240.
30. Chen YC, Wang YN, Hsu CH. Elucidating the dielectric properties of $Mg_2SnO_4$ ceramics at microwave frequency. *J Alloy Compd*. 2011;509:9650-9653.
31. Penn SJ, Alford NN, Templeton A, et al. Effect of porosity and grain size on the microwave dielectric properties of sintered alumina. *J Am Ceram Soc*. 1997;80:1985-1988.

**How to cite this article:** Zuo R, Zhang J, Song J, Xu Y. Liquid-phase sintering, microstructural evolution, and microwave dielectric properties of $Li_2Mg_3SnO_6$–LiF ceramics. *J Am Ceram Soc*. 2018;101:569–576. https://doi.org/10.1111/jace.15257